Journal of Marine Science and Technology; Vol. 18, No. 3; 2018: 256–268
DOI: 10.15625/1859-3097/18/3/12620
http://www.vjs.ac.vn/index.php/jmst

REMOTE SENSING DATA ANALYSIS WITH VALIDATION BY NUMERICAL MODEL FOR DETECTING SUSPENDED PARTICULATE MATTER CONCENTRATION IN COASTAL WATERS OF THE RED RIVER DELTA, VIETNAM

Nguyen Van Thao[1,*], Vu Duy Vinh[1], Do Thi Thu Huong[1], Chris Gouramanis[2]

[1]*Institute of Marine Environment and Resources, VAST, Vietnam*
[2]*Department of Geography, NUS, 21 Lower Kent Ridge Road, Singapore*
[*]E-mail: thaonv@imer.vast.vn

Received: 5-6-2018; accepted: 10-7-2018

Abstract. In this study, a set of optical and Suspended Particulate Matter data measured in the coastal waters of the Red river delta is examined to develop empirical and semi-analyzed algorithms to process satellite remote sensing data. A scene of high resolution satellite images of Landsat-8 OLI is used to test the algorithm for determining the distribution of Suspended Particulate Matter concentration in marine waters. A numerical model is also developed to calculate Suspended Particulate Matter transportation in the study area and calibrate statistics measured at certain monitoring stations of water flow and Suspended Particulate Matter from river discharged into the sea. The results on Suspended Particulate Matter concentrations in the coastal waters of the Red river delta determined from the satellite image algorithms and those of the numerical model are compared and evaluated.

Keywords: Remote sensing, algorithm, suspended particulate matter, Red river delta.

INTRODUCTION

The Red river is one of the largest rivers in Southeast Asia, originating from the Himalayas and contributes significant volumes of sediment to the world's oceans. The Red river contributes approximately 130×10^6 tons of sediment annually into the Tonkin Gulf via sixmain tributaries, with Van Uc (26% of total sediment), Thai Binh (11% of total sediment), Tra Ly (11% of total sediment), Ba Lat (26% of total sediment), Ninh Co (6% of total sediment) and Day (22% of total sediment) [1, 2]. During the rainy season in Northern Vietnam (July to November) 72% to 80% of the annual volume of sediment is discharged into the sea from the Red river. The Red river system plays an important role in the river - sea interaction and ecological processes in the coastal areas of Northern Vietnam. The distribution of Suspended Particulate Matter (*SPM*) in the coastal estuary is one of the important factors in evaluating the interaction between the river and sea over short and long time scales. SPM is also an important factor in the biogeochemical cycle in the coastal zone due to the varied chemistry contributed to the coastal environment. The determination of the *SPM* concentration in seawater is time-consuming, expensive and only provides information at the site of sample collection. In contrast, optical reflectance measured by satellite sensors can rapidly and economically assess SPM concentrations over large spatial areas in oceans, lakes, rivers and coastal waters [3, 4].

A drawback to using satellite-derived data is the requirement for robust and powerful algorithms to convert the radiation or reflection data measured by the satellite sensor into an accurate estimation of *SPM* concentration. For *SPM* measurements in coastal waters, it is necessary to modify the algorithms to accurately estimate the *SPM* concentration from data of ocean color remote sensing [5, 6]. Two algorithms (empirical and semi-analyzed) are often applied to obtain information on the water composition. Empirical and semi-analysis models are often used to develop data processing algorithms in order to determine the concentration of *SPM* in coastal areas. The empirical algorithm model is based on the assumption of existing relationship between the reflectance of water and *SPM* concentration [7–9]. The algorithm of the semi-analysis model is based upon the relationship between absorption and scattering of light in the visible band of the suspended particulate matter and their concentration [10–13].

In this study, the processing algorithms to identify the SPM concentration in the Red River coastal waters are developed based on both the empirical and the semi-analysis models. The results of the study are sigfinicant for the development and application of remote sensing in studying the sediment supply of rivers to oceans globally and for accurately investigating the spatial distribution and concentration of SPM in coastal marine systems.

MATERIALS AND METHOD

Materials

Optical data and SPM concentration. To calibrate the *SPM* concentration measured in the coastal waters with the reflectance data recorded in the satellite images, both reflectance and *SPM* concentrations were collected from the same sites along the coast of the Red river delta. The optical data and *SPM* concentrations were obtained from two field surveys in July 2014 at 21 sampling stations and June 2015 at 26 stations along the coastal area of Red river delta (fig. 1). The optical data was collected using a TRIOS with two automatic sensors that measured the radiance from the Sun and reflected from the water surface within the spectral range of 310–950 nm and with a resolution of 2 nm. The TRIOS was set up to collect a measurement every 10 seconds for 10 minutes for each station. The reflectance from the water (R_{rs}) is determined by the following equation:

$$R_{rs} = L_w / E_d \quad (1)$$

Where: L_w*:* Average value of the radiation from the water at each station; E_d*:* Average value of the direct solar radiation to the water surface at each station;

$$L_w = (L_{w1} + L_{w2} + \ldots + L_{w60})/60 \quad (2)$$

$$E_d = (E_{d1} + E_{d2} + \ldots + E\text{d}60)/60 \quad (3)$$

The Conductivity Temperature Depth (CTD) instrument was employed to automatically measure parameters such as water depth, temperature, salinity, turbidity and Chlorophyll-a at each station. The carbonate filter with 0.22 µm pore diameter were used to collect *SPM* samples. The *SPM* samples were measured using from quantity method and were performed at the Institute of Marine Environment and Resources.

Satellite image. Landsat-8 OLI satellite images of the Red river coastal area were obtained on 25 September, 2014 to calculate the *SPM* concentration. The images represent conditions that occur in the rainy (September) seasons in Northern Vietnam.

Data for the numerical model. The bathymetry and coastline in the Red river delta coastal area were digitized from topographic maps using VN2000 coordinates (Universal Transverse Mercator (UTM) projection with a WGS84 reference ellipsoid and specified local parameters) on the scale of 1:50,000 along the inner continental shelf and 1:25,000 in the estuary (data from the Ministry of Natural Resources and Environment, Vietnam). Offshore bathymetry was extracted from GEBCO-1/8 with 30 arc-second interval grid [14]. River water discharge was measured in 2014 at the river and was used to establish the boundary condition in the Red river. Winds and waves were measured at the stations of Hon

Dau, Bach Long Vi, Co To and Sam Son, and used in the calibration. Wind and wave data were measured for 6 hours in 2014 and used in this calibration. Sea levels were measured at the Hon Dau station and were used for model calibration and validation. From this location, the coastal sea levels were analyzed to determine the harmonic constants of eight tidal constituents (M2, S2, K2, N2, O1, K1, P1, Q1) for sea boundaries in the refined grid. The tidal offshore harmonic constants were extracted from FES 2014 [15, 16]. The coastal water *SPM* concentrations measured in the 2014 and 2015 surveys were also used for model calibration and validation. The World Ocean Atlas with 0.25 degree-grid resolution was used for the open sea boundary transport conditions of the parent model [17]. The *SPM* concentrations of the rivers were extracted from measured data of the national hydrometeorology sites of rivers of Cam, Van Uc, Tra Ly and Dao. They are average data of every flood and ebb tide dates within a year.

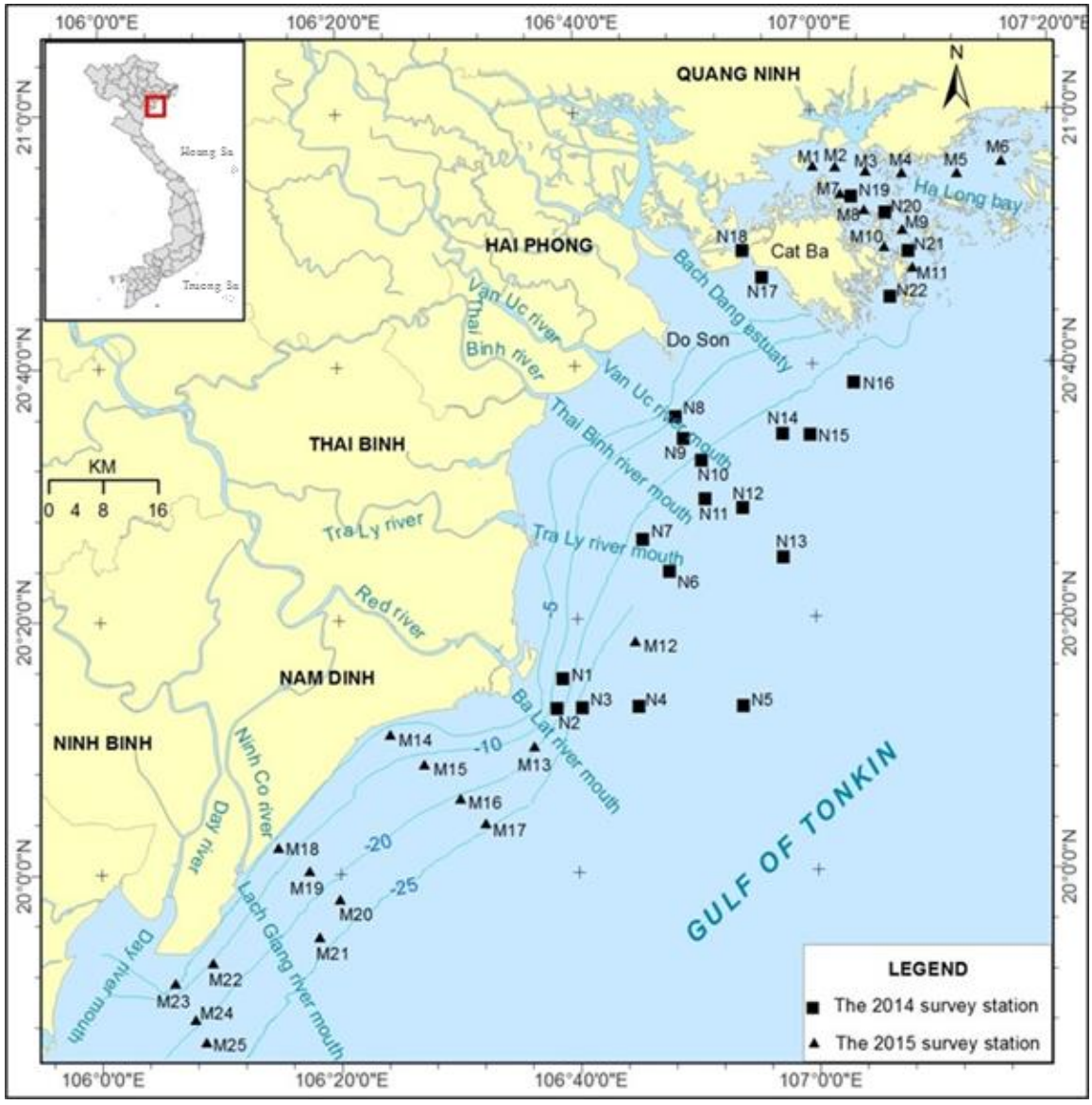

Fig. 1. Survey stations

Methods

Empirical algorithm. The empirical algorithm was developed by linear regression between water reflectance and the SPM concentration from the satellite red band when coefficient of determination (R^2) is maximised. Several studies show that the satellite red band can be used to detemine the relationship between the water reflectance and *SPM* concentration with field-surveyed data verification [18]. The optical data and SPM concentration from 47 survey points were used to determine the coefficient of determination. Six wavelengths (630, 640, 650, 660, 670 and 680 nm) in the red band were used to find out the maximum R^2. An atmospheric correction for Landsat8-OLI image was conducted based on MODTRAN model in the FLASH tool in the ENVI software. Reflectance values of terrestrial and tidal areas were assigined a factor of 0 when masking these areas. This step was necessary to reduce complexity as well as errors generated from reflectance spectra from the land during processing.

Semi-analyzed algorithm. The SPM concentration was determined from the satellite imagery by applying the equation developed by Nechad (2010):

$$SPM\ (\text{mg/l}) = A_T X\ R_{rs}/(1- R_{rs}/C) \qquad (4)$$

Where: R_{rs} is the water reflectance calculated by (1). A_T and C are correlation coefficients.

C has a negligible impact on the regression regime of the equation (4) because at wavelengths of red and infrared bands, C is large in comparison with water reflectance, e.g. R_{rs}/C approaches 0, and so (4) is simplified to $SPM \approx A_T X\ R_{rs}$. However, this is oversimplified (4) and C must be determined to ensure the accuracy of the equation (4). For increasing the accuracy of equation (4), it is necessary to add a standard deviation B_T, resulting in:

$$SPM\ (\text{mg/l}) = A_T X\ R_{rs}/(1- R_{rs}/C) + B_T \qquad (5)$$

To solve (5), A_T, C and B_T need to be determined by linearly regressing, but it is necessary to fix one of these parameters. Since C has a negligible impact on the regression regime, it is assigned a value determined by experimental measurement from the North Sea and South America [12].

Numerical model. Results of numerical models were used for validation of satellite processing with algorithms being developed in this study. Hydrodynamics (resulting from tides, currents and waves) and suspended sediment transport were simulated using the Delft3D-Flow and Delft3D-Wave modules [19]. The grid of the model is orthogonally curvilinear to provide a high grid resolution in the Red river delta and a low resolution elsewhere. The model frame includes entire coastal zone of the Red river Delta spanning 176 km west to east and 175 km north to south. The horizontal grid encompasses 608 × 605 points with grid size between 9.3 m and 1,800.3 m. Along the vertical direction, 5 layers in sigma coordinate are considered, like for the parent model. The hydrodynamic model included water temperature, salinity, sediment transport and wave action run with time steps of 30 s.

The model was calibrated for the periods of September 2014. River open boundaries for Bach Dang, Van Uc, Thai Binh, Tra Ly, Ba Lat, Lach Giang and Day were conditioned with time serial measurement of water river discharge, water temperature and SPM concentration.

For sea open boundaries, the forces of interest are tidal harmonic constants of each tidal constituent (M2, S2, K2, N2, O1, K1, P1, Q1) that were extracted from FES2004. The sea boundary transport conditions such as water temperature and sanity were determined with data from the WOA13 with 0.25 degree resolution. Wind velocity and direction measured every 6 hours in Bach Long Vi, Hon Dau, Co To and Sam Son gauging stations in 2014 were imposed on the model.

The wave module was established for online coupling with hydrodynamic and sediment transport at sea boundary conditions with data from the gauge stations located at Bach Long Vi, Co To and Sam Son. The bottom roughness of the inner shelf was specified by a spatial distribution of Manning (n) coefficients with values in the range 0.018–0.023 $m^{-1/3}$.s [20, 21]. The background horizontal eddy viscosity and horizontal eddy

diffusivity were considered to be, after calibration, equal to 8 $m.s^{-2}$.

The Horizontal Large Eddy Simulation (HLES) sub-grid, which is integrated in Delf3D-Flow, is based on theoretical values [22]. In this study, the HLES sub-grid was activated to add calculated results to background values. Two sediment fractions were simulated in the model: One non-cohesive and one cohesive. Measured grain sizes of non-cohesive particles in the Red river delta coastal area range from 85 μm to 406 μm, average 135 μm [23]. A specific density of 2,650 $kg.m^{-3}$ and dry bed density of 1,600 $kg.m^{-3}$ were considered; all other sand transport calibration parameters were kept at the default values proposed by Delft-3D. Sand fraction transport was modeled with the van Rijn TR2004 formulation [24], which has been shown to successfully represent the movement of non-cohesive sediment ranging in size from 60 μm to 600 μm. If the bed shear stress is larger than a critical value, erosion is modeled following the Partheniades' formulation [25] while if the bed shear stress is less than a critical value for deposition, Krone's formula [26] is used to quantify the deposition flux. The parameters required to simulate the cohesive sediment transport include critical bed shear stresses for erosion τ_{cre} and deposition τ_{crd}, the erosion parameter M and the particle settling velocity w_s [27]. After calibration, τ_{crd} was set to 1,000 $N.m^{-2}$, which effectively implied that deposition was a function of concentration and fall velocity [28]. τ_{cre} was set to 0.2 $N.m^{-2}$, and M was set to 2×10^{-5} $kg.m^{-2}.s^{-1}$.

For salt water, cohesive sediments flocculate, the degree of flocculation depends on salinity. Flocs are much larger than the individual sediment particles and settle at a faster rate. In order to model this salinity dependency, Delft3D-Flow considers two settling velocities and a maximum salinity. The velocity $w_{s,f}$ is the settling velocity of the sediment fraction in fresh water (salinity S = 0), while the velocity $w_{s,max}$ is the settling velocity of the cohesive fraction in water having an equally salinity to salmax (S = 30 over our area). Portela et al., 2013 reported settling velocities to increase by a factor of 6.5 between freshwater conditions (S = 0) and marine conditions (S = 30). In this study, the settling velocity of the cohesive sediments was set to 0.05 $mm.s^{-1}$ in fresh water and to 0.325 $mm.s^{-1}$ at S = 30. The bottom-boundary layer accounts for the interaction of wave and current over a moveable bed [30].

RESULTS

Empirical algorithm for the coastal area of Red River Delta. To maximise R^2 between the R_{rs} and *SPM* concentration, the linear, logarithmic, natural logarithm (ln), exponentiation and polynomial functions were tested for six different wavelengths. The quadratic polynomial function at the wavelength of 650 nm produced the largest R^2 (0.903, fig. 2).

This was expected because after atmospheric correction, the R_{rs} of the red band of the Landsat-8 OLI image is equivalent to the 650 nm wavelength, and corresponds to the central wavelength within the red band of the Landsat-8 OLI image (0.636–0.673 nm). The polynomial derived from the 650 nm wavelength is:

$$SPM\left(mg/l\right) = 64,595XR_{rs}^2 + 127.8XR_{rs} + 1.256 \quad (6)$$

Semi - analyzed algorithm for the coastal area of the Red river delta. The high R^2 and lowest Root Mean Squared Error (RMSE) between R_{rs} and *SPM* concentration at the wavelength of 650 nm using (5) produces the best estimates of A_T and B_T (table 1).

Thus, at the wavelength of 650 nm, the value of A_T and B_T are 1,030 mg/l and -0.5275 mg/l, respectively (table 1). Hence, equation (5) is redefined as:

$$SPM\left(mg/l\right) = 1,030XR_{rs}/\left(1 - R_{rs}/0.1661\right) - 0.5275 \quad (7)$$

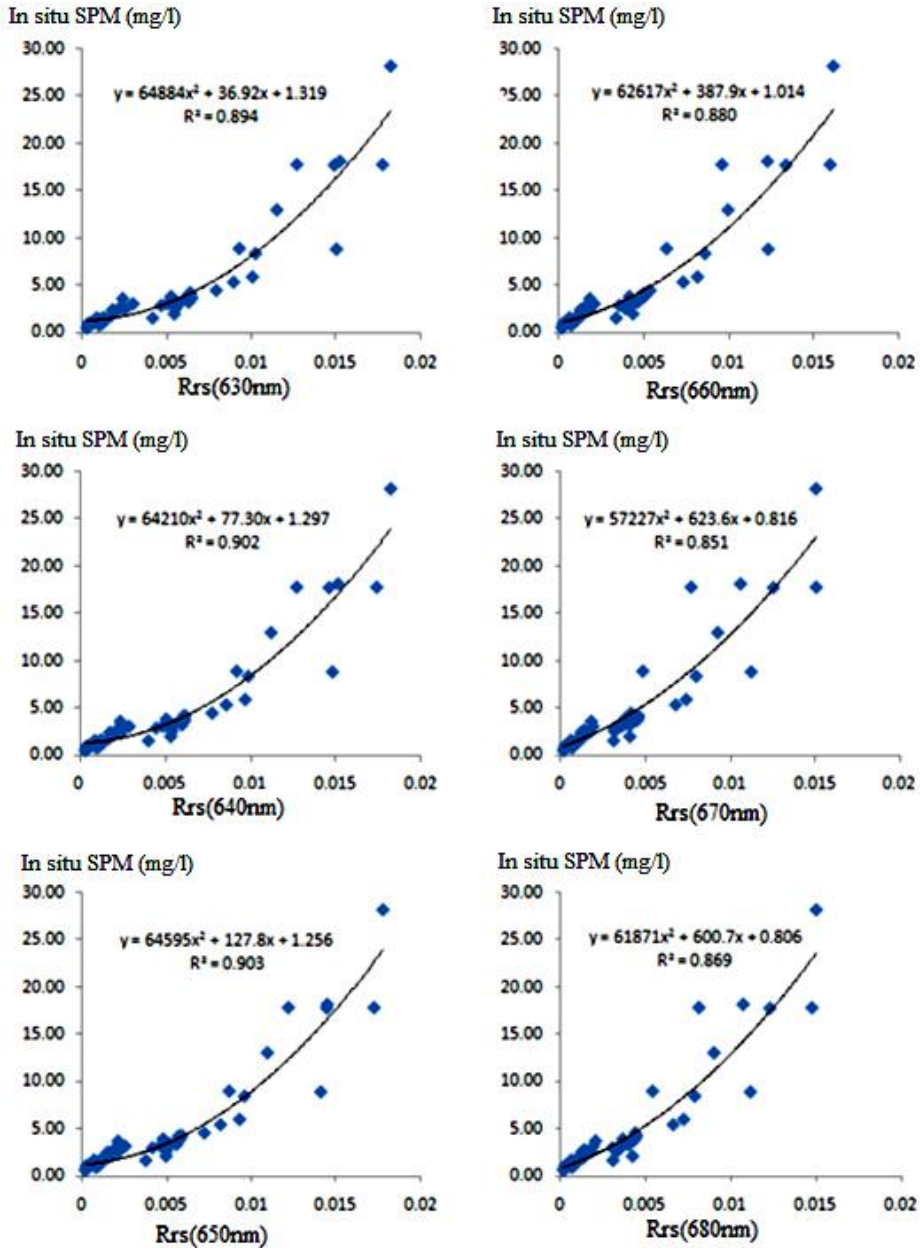

Fig. 2. The correlation of R_{rs} and *SPM* concentration according to polynomial function at different wavelengths of the red band

Table 1. The results of A_T and B_T calculation

Wavelength (λ)	A_T	B_T	R^2	RMSE
630 nm	975.5	-0.6691	0.8321	2.456
640 nm	997.4	-0.5994	0.8436	2.37
650 nm	1030	-0.5275	0.8487	2.332
660 nm	1171	-0.366	0.8463	2.35
670 nm	1280	-0.2722	0.8308	2.466
680 nm	1312	-0.3707	0.8463	2.35

Calibration and validation for numerical model. The calibration and validation of the tidal model were tested using the Nash-Sutcliffe efficiency coefficient *E* [31]:

$$E = 1 - \frac{\sum(obs - calc)^2}{\sum(obs - mean)^2} \quad (8)$$

Where: *obs*= the observed value and *calc*= the model calculated value. *E* values range from 0 (no correlation) to 1 (perfect correlation). As such high *E* implies a good fit between the model and the data. The discrepancy between model results and field measurements in dry and flood seasons of 2012, flood of 2013 and dry season 2014 was quantified. After calibration, the model and observed results show good agreement with *E* ranging from 0.77 to 0.82. The measured SPM and modeled SPM (fig. 3c) also show excellent agreement with R^2 of 0.89.

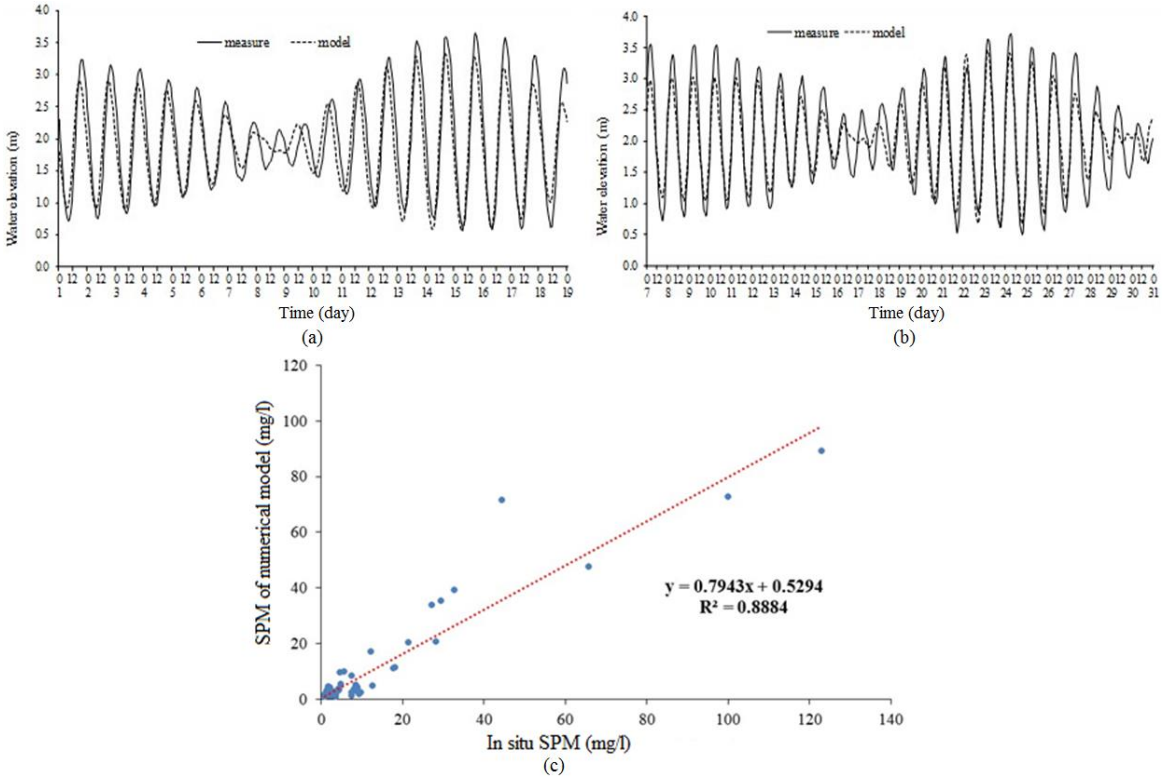

Fig. 3. The result on calibration and validation of numerical model

SPM concentration from Landat-8 OLI. Using equations 6 and 7 to calculate the *SPM* concentration for each pixel of satellite images after atmospheric correction and converting DN value into R_{rs} values. The results of the *SPM* concentration using band 4 of Landsat-8 OLI images on 25 September 2014 (fig. 4) show the concentration of *SPM* in the Red river coastal area. During the rainy season, high concentrations of *SPM* occur near the river mouths with river discharge and nearshore currents moving the *SPM* to the south and southeast of the river mouths (fig. 4). The processing of the 25 September, 2014 Landsat-8 OLI image shows that *SPM* concentrations along the coastal area of the Red river delta is high (over 20 mg/l), especially at Day, Lach Giang, Ba Lat, Tra Ly, Thai Binh and Van Uc river mouths. In marine waters deeper than 15 m, the *SPM* concentration is low, ranging from 1 mg/l to 15 mg/l.

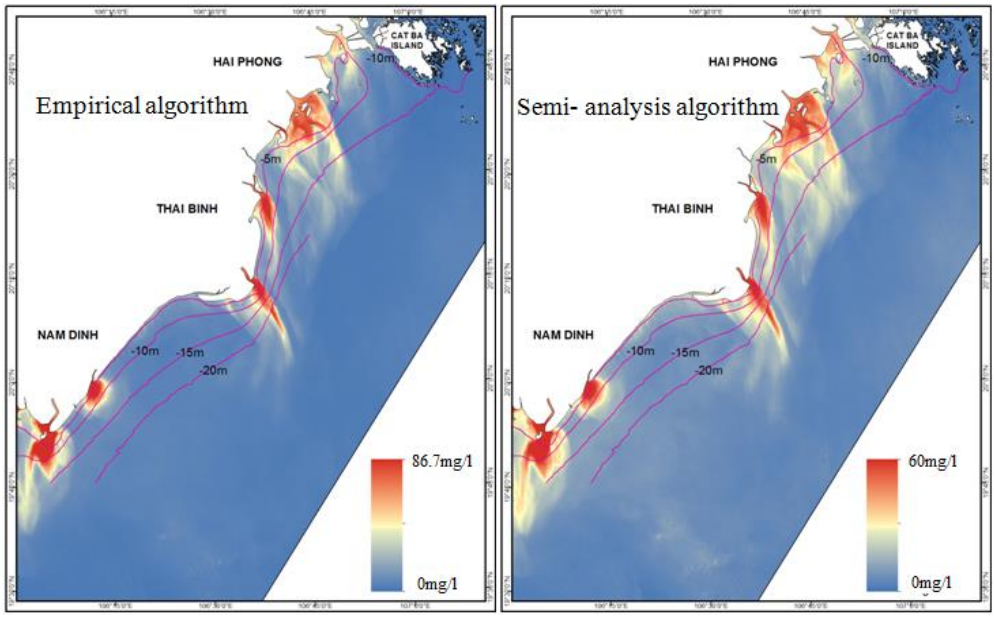

Fig. 4. SPM concentration from Landsat-8 OLI image on September, 25th, 2014

Validation of algorithms. The best way to assess the accuracy of satellite image processing is to compare the satellite-derived results with in situ, measured data. However, this is difficult because the *SPM* concentration at a site can significantly and rapidly change with time due to oceanographic and climatic conditions (e.g. wave, currents, tides). Satellite images are also captured very quickly and so provide an instantaneous record of the oceanic conditions. Therefore, it is very difficult to obtain real time data that corresponds with the time when a satellite image is obtained. To solve this problem, we used the results of the *SPM* concentration distribution extracted from the numerical model calculated at the same time as the Landsat-8 OLI image was obtained. Three 20 km long profiles with 20 equally-spaced sampling points along each profile were used to extract *SPM* concentrations from the satellite images to compare and evaluate the satellite image processing and the numeric model.

The trends of the *SPM* concentrations extracted from the Landsat-8 OLI images and those calculated from the numerical model agree despite some differences in the absolute values at some locations along the profiles. For example, the value of *SPM* concentration extracted from Landsat-8 OLI obtained on 25 September 2014 based on the empirical algorithm ranges between being very similar to the numerical model and semi-analyzed algorithm along the Bach Dang river mouth profile. Along the Ba Lat river profile the empirical algorithm calculates much higher *SPM* concentrations near the river mouth than the numerical model or semi-analyzed algorithm does, but the *SPM* concentration estimates of the three methods converge further offshore (fig. 5). The reverse is observed from the Day river profile with similar *SPM* concentration estimates observed near the river mouth and the empirical algorithm estimates deviating from the numerical model and semi-analyzed algorithm as water depth increases (fig. 5).

Regression modelling was used to assess the errors between the *SPM* concentration estimates extracted from the Landsat-8 OLI algorithms and the numeric model. The *SPM* concentrations of 60 estimates from the profiles (20 estimates from each profile) were selected to assess the relationship between the satellite derived algorithm estimates and the estimates from the numerical model. The results show the good agreement between *SPM* concentrations extracted from satellite images based on algorithms and the numerical model with R^2

over 0.868 (fig. 6). Thus, there is a high correlation between the result of *SPM* concentration extracted from satellite image and that of numeric model.

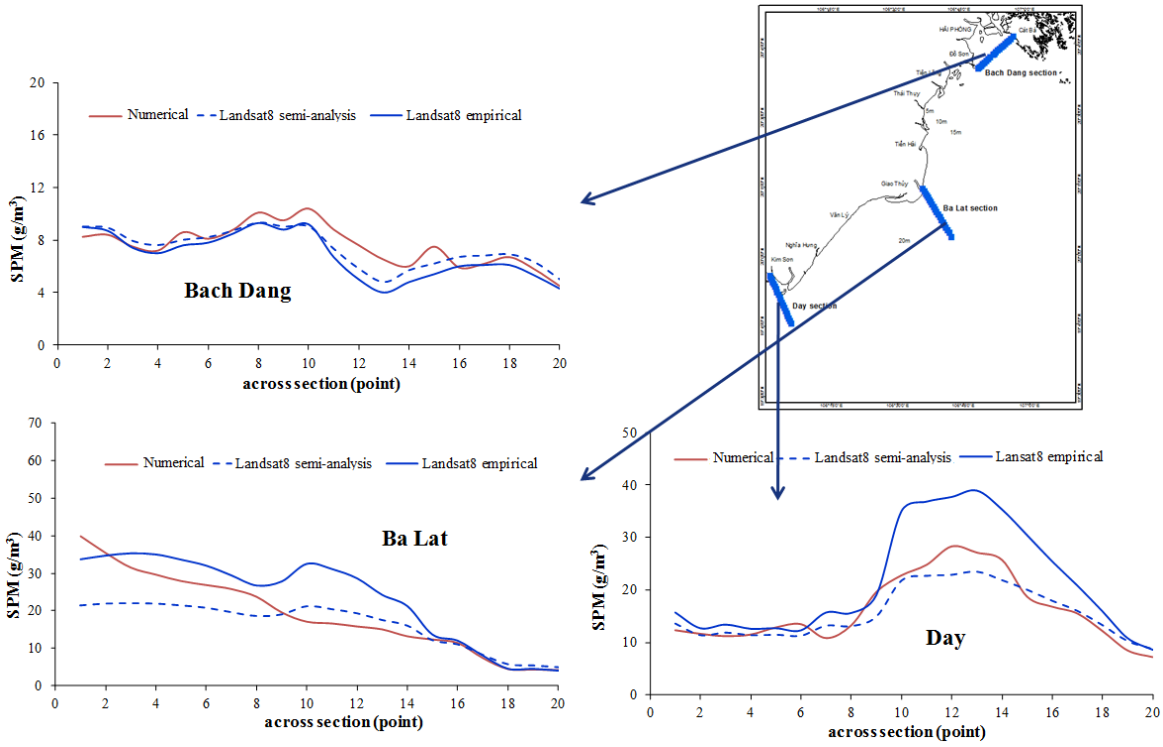

Fig. 5. The comparison of results on SPM concentration extracted from Landsat-8 OLI processing and numeric model on 25 September 2014

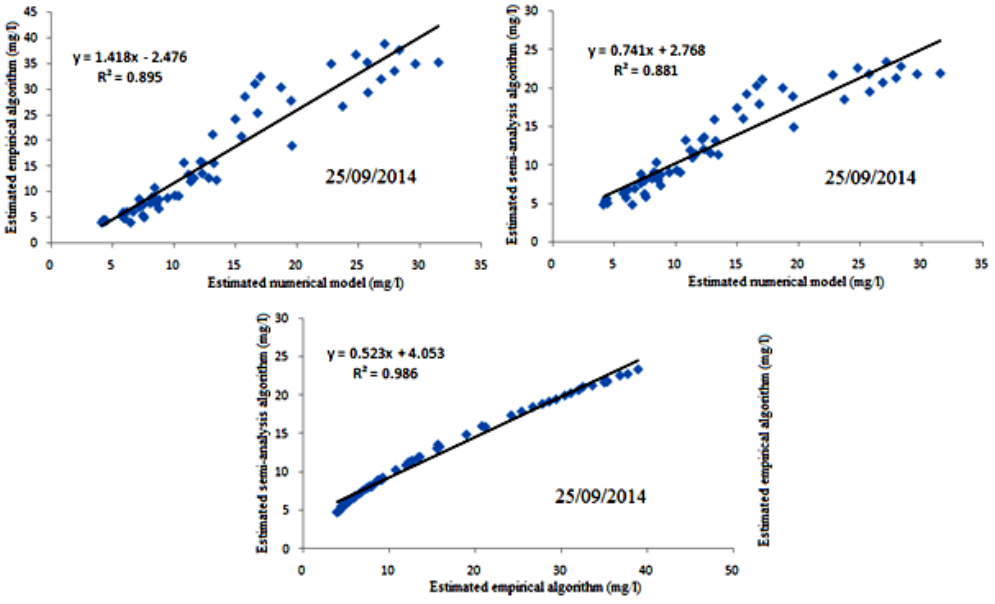

Fig. 6. Comparison of relationship coefficient of SPM concentrations extracted from Landsat-8 OLI processing and numeric model at 03 sections

DISCUSSION

It has been demonstrated that experimental algorithms can be used to obtain spatial information on water composition (optical properties, *SPM* concentration) from the reflectance of the sea surface. The relationship between the *SPM* concentration of coastal waters and the reflectance of coastal waters shows that algorithms derived from the reflectance of a single optical band produce the best relationships for identifying *SPM* concentrations and spatial distributions [32, 33]. Nechand et al., (2010) proposed a single band algorithm for total suspended solids obtained from the reflection pattern and correction of the results using reflectance measured from aircraft and total suspended solids measured in the southern part of the North Sea. The optical properties of water and suspended sediment are nonlinear and the relationship is affected by the size, shape and color of the suspended particles [34–37]. Due to the complex optics, it is difficult to define a universal algorithm to estimate the *SPM* concentration from satellite images [38]. Moreover, various parameters such as coastal geomorphology, variable river flow, local and seasonal coastal and oceanic circulation variability affect the distribution of *SPM* concentration. Therefore, the algorithms developed for a certain area can not be applied to other areas. The result of the calculated *SPM* concentrations in the coastal zone of the Red river delta from remotely sensed data is comparable to studies on *SPM* concentration and spatial distributions performed elsewhere [39–41]. The results show that *SPM* concentrations are higher during the peak of the wet season (September) causing a high volume of sediment to be discharged into the coastal area of the Red river delta [42]. However, the result from empirical algorithm is limited by its isolated capacity [12]. That does not separate the water reflectance of inorganic, organic particles, water and the bottom of the coastal areas, leading to certain errors when calculating the *SPM* concentration. Adding to the complexity of components contributing to water reflectance, the Red river tributaries produce many submerged offshore bars [43]. These bars increase the variability of the water depth, and as the 25 September 2014 satellite image was obtained during the neap tide (1.67 m), the shallow water increases the contribution of bottom sediments to water reflectance. Although wave height was minimal when the 25 September 2014 satellite image was collected, the shallow water of the neap tide resulted in further bottom sediment disturbance affecting the water reflectance.

CONCLUSION

Empirical models with algorithms of satellite data processing to determine *SPM* concentration are developed based on the function of quadratic polynominal with (R^2) correlation coefficient over 0.9 derived from the relationship between the water-leaving reflectance at wavelength of 650 nm and *SPM* concentration of 47 survey stations at the coastal area of Red river delta in 2014 and 2015. Semi-analyzed models with its algorithm developed using the equation of Nechad (2010) are made at the wavelength of 650 nm, and the parameters A_T = 1,030 mg/l and B_T = -0.5275 mg/l. Validation results of algorithm with numeric model of linear correlation coefficient between the results of the calculated *SPM* and actual measurements at factor of 0.89 and Nash -Sutcliffe of 0.87 are highly compatible. However, to increase the accuracy of the algorithm, it is necessary to have series of in situ measured data and real time measurements.

Acknowledgement: This is made available with supports from the bilateral cooperation project between Vietnam and China "Comparative study of Holocene sedimentary evolution of the Red river delta and Yangtze river delta".

REFERENCES

[1] Milliman, J. D., and Syvitski, J. P., 1992. Geomorphic/tectonic control of sediment discharge to the ocean: the importance of small mountainous rivers. *The Journal of Geology*, **100**(5), 525–544.

[2] Pruszak, Z., Van Ninh, P., Szmytkiewicz, M., Hung, N. M., and Ostrowski, R., 2005. Hydrology and morphology of two river mouth regions (temperate Vistula

Delta and subtropical Red river delta). *Oceanologia*, **47**(3), 365–385.

[3] Mckim, H. L., Merry, C. J., and Layman, R. W., 1984. Water quality monitoring using an airborne spectroradiometer. *Photogrammetric Engineering and Remote Sensing*, **50**, 353–360.

[4] Curran, P. J. and Wilkinson, H. D., 1985. Mapping the concentration and dispersal pattern of dye from a long sea outfall using digitized aerial photography. *Journal of Remote Sensing*, **6**, 17–31.

[5] Robinson, M. C., Morris, K. P., and Dyer, K. R., 1999. Deriving fluxes of suspended particulate matter in the Humber estuary, UK, using airborne remote sensing. *Marine Pollution Bulletin, 37*(3–7), 155–163.

[6] Moore, G. F., Aiken, J., and Lavender, S. J., 1999. The atmospheric correction of water colour and the quantitative retrieval of suspended particulate matter in Case II waters: application to MERIS. *International Journal of Remote Sensing*, **20**(9), 1713–1733.

[7] Forget, P., and Ouillon, S., 1998. Surface suspended matter off the Rhone river mouth from visible satellite imagery. *Oceanologica Acta*, **21**(6), 739–749.

[8] Doxaran, D., Froidefond, J. M., and Castaing, P., 2002. A reflectance band ratio used to estimate suspended matter concentrations in sediment-dominated coastal waters. *International Journal of Remote Sensing*, **23**(23), 5079–5085.

[9] Ouillon, S., Douillet, P., Petrenko, A., Neveux, J., Dupouy, C., Froidefond, J. M., Andréfouët, S., and Muñoz-Caravaca, A., 2008. Optical algorithms at satellite wavelengths for total suspended matter in tropical coastal waters. *Sensors*, **8**(7), 4165–4185; doi:10.3390/s8074165.

[10] Chen, Z., Hu, C., and Muller-Karger, F., 2007. Monitoring turbidity in Tampa Bay using MODIS/Aqua 250 m imagery. *Remote sensing of Environment*, **109**(2), 207–220.

[11] Doxaran, D., Froidefond, J. M., Castaing, P., and Babin, M., 2009. Dynamics of the turbidity maximum zone in a macrotidal estuary (the Gironde, France): Observations from field and MODIS satellite data. *Estuarine, Coastal and Shelf Science*, **81**(3), 321–332.

[12] Nechad, B., Ruddick, K. G., and Park, Y., 2010. Calibration and validation of a generic multisensor algorithm for mapping of total suspended matter in turbid waters. *Remote Sensing of Environment*, **114**(4), 854–866.

[13] Dogliotti, A. I., Ruddick, K. G., Nechad, B., Doxaran, D., and Knaeps, E., 2015. A single algorithm to retrieve turbidity from remotely-sensed data in all coastal and estuarine waters. *Remote Sensing of Environment*, **156**, 157–168.

[14] Weatherall, P., Marks, K. M., Jakobsson, M., Schmitt, T., Tani, S., Arndt, J. E., Rovere. M., Chayes, D., Ferrini, V., and Wigley, R., 2015. A new digital bathymetric model of the world's oceans. *Earth and Space Science*, **2**(8), 331–345. doi:10.1002/2015EA000107.

[15] Lefevre, F., Lyard, F. H., Le Provost, C., and Schrama, E. J., 2002. FES99: a global tide finite element solution assimilating tide gauge and altimetric information. *Journal of Atmospheric and Oceanic Technology*, **19**(9), 1345–1356.

[16] Lyard, F., Lefevre, F., Letellier, T., and Francis, O., 2006. Modelling the global ocean tides: modern insights from FES2004. *Ocean Dynamics*, **56**(5-6), 394–415.

[17] World Ocean Atlas 2013 version 2 (WOA13 V2). Available online: https://www.nodc.noaa.gov/OC5/woa13/ (accessed 20-04-2016).

[18] Sravanthi, N., Ramana, I. V., Yunus Ali, P., Ashraf, M., Ali, M. M., and Narayana, A. C., 2013. An algorithm for estimating suspended sediment concentrations in the coastal waters of India using remotely sensed reflectance and its application to coastal environments. *International Journal of Environmental Research*, **7**(4), 841–850.

[19] Hydraulics, D., 2014. Delft3D-FLOW User Manual: Simulation of multi-dimensional hydrodynamic flows and transport phenomena. including

sediments. Technical report; Available online: http://oss.deltares.nl/documents/183920/185723/Delft3D-FLOW_User_Manual.pdf (accessed 20-04-2016).

[20] Schneider, V. R., and Arcement, G. J., 1989. Guide for Selecting Manning's Roughness Coefficients for Natural Channels and Flood Plains. *Available from the US Geological Survey, Books and Open-File Reports Section, Box 25425, Federal Center, Denver, CO 80225-0425. Water-Supply Paper 2339, 1989.* 38 p, *22 fig., 4 tab., 23 ref.*

[21] Simons, D. B., and Şentürk, F., 1992. Sediment transport technology: water and sediment dynamics. *Water Resources Publication*.

[22] Uittenbogaard, R. E., 1998. Model for eddy diffusivity and viscosity related to sub-grid velocity and bed topography. *Note, WL| Delft Hydraulics*.

[23] Duc, D. M., Nhuan, M. T., Ngoi, C. V., Nghi, T., Tien, D. M., van Weering, T. C., and van den Bergh, G. D., 2007. Sediment distribution and transport at the nearshore zone of the Red River delta, Northern Vietnam. *Journal of Asian Earth Sciences*, **29**, 558–565.

[24] Van Rijn, L. C., 2007. Unified view of sediment transport by currents and waves. I: Initiation of motion, bed roughness, and bed-load transport. *Journal of Hydraulic Engineering*, **133**(6), 649–667; doi:10.1061/(ASCE)0733-429(2007)133:6(668).

[25] Partheniades, E., 1965. Erosion and deposition of cohesive soils. *Journal of the Hydraulics Division*, **91**(1), 105–139.

[26] Krone, R. B., 1962. Flume studies of the transport of sediment in estuarial shoaling processes, final report, Hydraul. *Eng. Lab. and Sanit. Eng. Res. Lab., Univ. of Calif., Berkeley*.

[27] Douillet, P., Ouillon, S., and Cordier, E., 2001. A numerical model for fine suspended sediment transport in the southwest lagoon of New Caledonia. *Coral Reefs*, **20**(4), 361–372; doi: 10.1007/s00338-001-0193-6.

[28] Winterwerp, J. C., and Van Kesteren, W. G., 2004. Introduction to the physics of cohesive sediment dynamics in the marine environment (Vol. 56). *Elsevier*. 576 p. eBook ISBN: 9780080473734; Hardcover ISBN: 9780444515537.

[29] Portela, L. I., Ramos, S., and Teixeira, A. T., 2013. Effect of salinity on the settling velocity of fine sediments of a harbour basin. *Journal of Coastal Research*, **65**(sp2), 1188–1193.

[30] Walstra, D. J. R., Roelvink, J. A., and Groeneweg, J., 2001. Calculation of wave-driven currents in a 3D mean flow model. In *Coastal Engineering 2000* (pp. 1050–1063); doi:10.1061/40549(276)81.

[31] Nash, J. E., and Sutcliffe, J. V., 1970. River flow forecasting through conceptual models part I-A discussion of principles. *Journal of Hydrology*, **10**(3), 282–290. doi:10.1016/0022-1694(70)90255-6.

[32] Curran, P. J., Hansom, J. D., Plummer, S. E., and Pedley, M. I., 1987. Multispectral remote sensing of nearshore suspended sediments: a pilot study. *International Journal of Remote Sensing*, **8**(1), 103–112.

[33] Novo, E. M. M., Hansom, J. D., and Curran, P. J., 1989. The effect of viewing geometry and wavelength on the relationship between reflectance and suspended sediment concentration. *International Journal of Remote Sensing*, **10**(8), 1357–1372.

[34] Baker, E. T., and Lavelle, J. W., 1984. The effect of particle size on the light attenuation coefficient of natural suspensions. *Journal of Geophysical Research: Oceans*, **89**(C5), 8197–8203.

[35] Curran, P. J., and Novo, E. M. M., 1988. The relationship between suspended sediment concentration and remotely sensed spectral radiance: a review. *Journal of Coastal Research*, **4**(3), 351–368.

[36 Stumpf, R. P., and Pennock, J. R., 1989. Calibration of a general optical equation for remote sensing of suspended sediments in a moderately turbid estuary. *Journal of Geophysical Research: Oceans*, **94**(C10), 14363–14371.

[37] Sydor, M., and Arnone, R. A., 1997. Effect of suspended particulate and

dissolved organic matter on remote sensing of coastal and riverine waters. *Applied Optics*, **36**(27), 6905–6912.

[38] Lee, Z. P., 2006. Remote sensing of inherent optical properties: Fundamentals, tests of algorithms, and applications, Rep. 5, 126 p. Int. Ocean-Colour Coord. *Group, Dartmouth, NS, Canada*.

[39] Häglund, M., and Svensson, P., 2002. Coastal Erosion at Hai Hau Beach in the Red river delta, Vietnam. *Lund, Sweden: Lund University* (*Doctoral dissertation, Master's thesis*).

[40] Te Slaa, S., 2009. Coastal erosion processes near sea dikes in Hai Hau district, Vietnam. *Master thesis in Delft University of Technology*.

[41] Van Maren, D. S., 2004. Morphodynamics of a Cyclic Prograding Delta: The Red River, Vietnam. *Utrecht, the Netherlands: Utrecht University* (*Doctoral dissertation, Doctoral thesis*). 167 p.

[42] Vinh, V. D., and Ouillon, S., 2014. Effects of Coriolis force on current and suspended sediment transport in the coastal zone of Red River Delta. *Journal of Marine Sceince and Technology*, **14**(3), 219–228.

[43] Van Maren, D. S., 2007. Water and sediment dynamics in the Red River mouth and adjacent coastal zone. *Journal of Asian Earth Sciences*, **29**(4), 508–522.